Supplementary Information

N, S-doped hollow carbon nanosheet encapsulated Co_9S_8 nanoparticles as high-efficient bifunctional electrocatalyst for rechargeable zinc-air battery

Yuanyuan Peng ‡[a], Fuping Zhang ‡[a], Yinglin Zhang [a], Xing Luo [a], Long Chen [a]*, Yulin Shi [a,b]*

[a] Key Laboratory for Green Processing of Chemical Engineering of Xinjiang Bingtuan, School of Chemistry and Chemical Engineering, Shihezi University, Shihezi 832003, China

[b] Bingtuan Industrial Technology Research Institute, Shihezi University, Shihezi 832003, PR China

‡These authors contributed equally to this work.

*Corresponding authors.

E-mail: shiyulin521@126.com (Y. Shi), chenlong2012@sinano.ac.cn (L. Chen).

1. Experiment Section

1.1 Physical Characterizations

The surface morphologies and microstructures were studied by Scanning electron microscopic (SEM; Zeiss Sigma 300, 3 KV, Germany), transmission electron microscopy(TEM), high-resolution TEM (HRTEM), and element mapping (JEOL, JEM2100PLUS, 200 kV, Japan). X-ray diffraction (XRD) patterns were conducted on a Bruker D8 (Germany) apparatus with Cu-K α radiation at scan rate of 8˚/min. Raman spectra were collected under a laser excitation of 514 nm by a Raman microscope (Renishaw, England). The chemical composition and configuring of different elements

were determined by X-ray photoelectron spectroscopy (XPS, Thermo Scientific K-Alpha, USA) apparatus. The binding energies were calibrated by employing the C 1s peak at 284.8 eV as the reference.

1.2 ORR and OER performance Measurements

ORR and OER related measurements were tested on CHI 760E (CHI Instruments) in a standard three-electrode system. A polished glassy carbon electrode (3 mm) loaded with catalyst was used as the working electrode, a graphite rod as the counter electrode and a Hg/HgO (1.0 M KOH) electrode as the reference electrode. All the measured potentials were converted to the reversible hydrogen electrode (RHE) by Eq (S1) [1]:

$$E(\mathrm{RHE}) = E(Hg/HgO) + 0.0591\ \mathrm{pH} + 0.098 \quad \text{(S1)}$$

To prepare the working electrode, the catalyst powder (3 mg) was dispersed in a mixture of Nafion® dispersion (20 μL) and ethanol solution (480 mL) via continuous sonication for 60 min to form a homogeneous catalytic ink. Then, 7 μL of catalyst ink was placed on the glass carbon electrode with a mass loading of ~0.59 mg cm^{-2}. As comparison, the Pt/C catalyst and RuO_2 catalyst inks were also prepared with a mass loading of ~ 0.2 mg cm^{-2}, respectively.

The ORR performance was investigated in N_2/O_2-saturated 0.1 M KOH solution, the cyclic voltammetry (CV) curves were collected at 50 mV s^{-1} and the linear sweep voltammetry (LSV) curves were conducted under varying rotating speeds (400-2500 rpm) at a scan rate of 5 mV s^{-1}. The Koutechy-Levich equations shown below [Eqs. (S2), (S3) [2]] were used to analyze the transferred electron numbers (n):

$$\frac{1}{J} = \frac{1}{J_K} + \frac{1}{J_L} = \frac{1}{J_K} + \frac{1}{B\omega^{0.5}} \quad \text{(S2)}$$

$$B = 0.62nF(D_{O_2})^{2/3}C_{O_2}\nu^{-1/6} \quad \text{(S3)}$$

where J represents the measured current density and J_K represents the kinetic current density, ω indicates the angular velocity of the glassy carbon electrode, F is the Faraday constant (96485 C mol^{-1}), D_{O2} is the diffusion coefficient of O_2 (1.9×10^{-5} cm^2 s^{-1}), ν is the kinematic viscosity of the electrolyte (0.01 cm^2 s^{-1}), and C_{O2} is the concentration of O_2 (1.2×10^{-6} mol cm^{-3}).

The rotating ring disk electrode (RRDE) measurements were implemented to determine the electron transfer number (n) and the peroxide percentage $HO_2^-\%$. The equations are as follows [Eqs. (S4), (S5) [3]].

$$n = \frac{4 \times i_d}{i_d + \frac{i_r}{N}} \quad \text{(S4)}$$

$$HO_2^-\% = \frac{200 \times \frac{i_r}{N}}{i_d + \frac{i_r}{N}}\% \quad \text{(S5)}$$

Where i_d and i_r are the disk and ring current, respectively, and N=0.37 is the current collection efficiency of the Pt ring.

The stability tests were implemented through current-time (i-t) chronoamperometric responses for 0.5 V (vs. RHE) for 30000 s and methanol tolerance tests were collected by i-t response at the above potential with 4 mL methanol (3 M) addition at 500 s.

The OER performance was also investigated by LSV curves in 0.1 M KOH with

a scan rate of 5 mV s^{-1} and rotating speed of 1600 rpm. The 80% iR-compensation was employed. To better understand the performance of overall oxygen electrode activity, ΔE was estimated as follows [Eqs. (S6) [4]]

$$\Delta E = E_{OER,10} - E_{ORR,1/2} \quad \text{(S6)}$$

The Tafel slope was obtained in a potential region, in which the current was fully controlled by catalytic kinetics, based on the Tafel equation: $\eta=a+b\cdot Log(j)$ [5]. Where, b is the Tafel slope, η and j are in turn the overpotential and the current density, and a represents the intercept, which is related to the exchange current density. The electrochemical impedance spectroscopy (EIS) tests were performed in a frequency range from 100 kHz to 0.01 Hz with AC amplitude of 5 mV at 1.5 V vs RHE. To obtained electrochemical surface area (ECSA) and double-layer capacitance (C_{dl}), the CV curves were measured in the non-Faradaic region (1.1-1.2 V vs. RHE) with the scan rates of 5, 10, 15, 20, 25, 30, 35, and 40 mV s^{-1}. The C_{dl} values were obtained by fitting the plot of $(J_a-J_c)/2$ at 1.15 V (vs. RHE) at various scan rates, in which J_a presents anodic current density and J_c presents cathodic current density. The long-term stability tests were assessed by chronoamperometry responses for 1.4 V (vs. RHE) for 20000 s at potential at 10 mA cm^{-2}. The accelerated degradation test (ADT) was carried out using CV from 1.4 V to 1.5 V at 100 mV s^{-1} and the LSV curve was recorded before and after 5000 cycles. The turnover frequency (TOF) values were calculated from the formula [6]

$$TOF=JA/4Fn \quad \text{(S7)}$$

where J is the current density (A cm^{-2}) at various overpotentials, A is the area of the electrode, 4 implies four electrons per mol of O_2, F is the Faraday constant (96485

C mol^{-1}), and n is the number of moles of active sites.

1.3 Zinc-Air Battery Tests

The air electrode was constructed by pressing the catalyst layer (CL) on of the nickel foam substrate at 10 MPa. The CL was prepared via ultrasonically mixing the catalyst power (Co_9S_8/NSC_{-3}) (2 mg), Nafion® dispersion (20 μL) and ethanol solution (480 mL) for 60 min followed by dropping in nickel foam (1 cm×1 cm) and dried at 80 °C for 12 h. The mass loading of Co_9S_8/NSC_{-3} was 2 mg cm^{-2}. For comparison, a hybrid catalyst of commercial Pt/C (1 mg) and RuO_2 (1 mg), labeled as Pt/C+RuO_2, was also prepared. The zinc-air battery (ZAB) was assembled with the as-prepared air electrode as the cathode, Celgard 2340 membrane as a separator, a polished Zn plate (0.3 mm thickness) as the anode, and 6 M KOH containing 0.2 M $Zn(Ac)_2 \cdot 2H_2O$ as the electrolyte. All the electrochemical measurements of ZABs were conducted using the electrochemical workstation (CHI 760E, Shanghai) under ambient atmosphere.

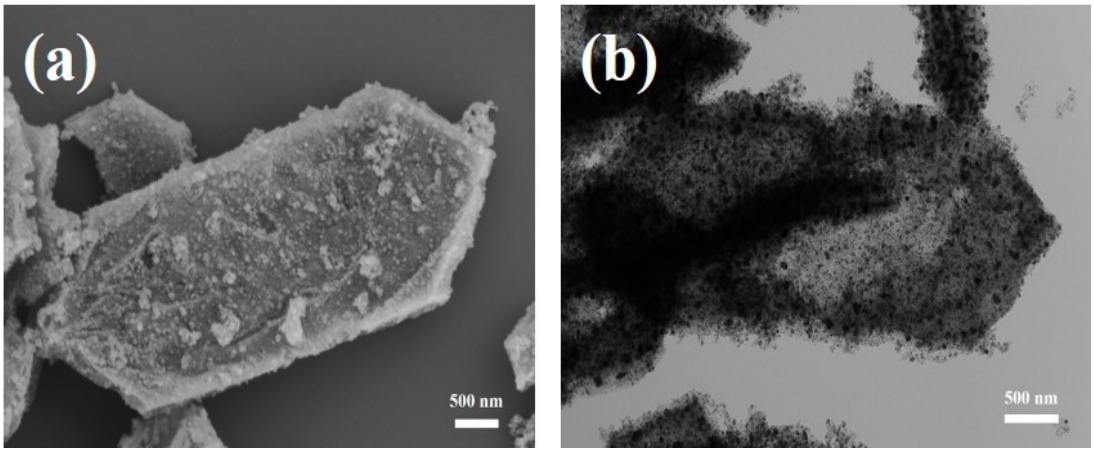

Fig. S1 (a) SEM image and (b) TEM image of CoNC.

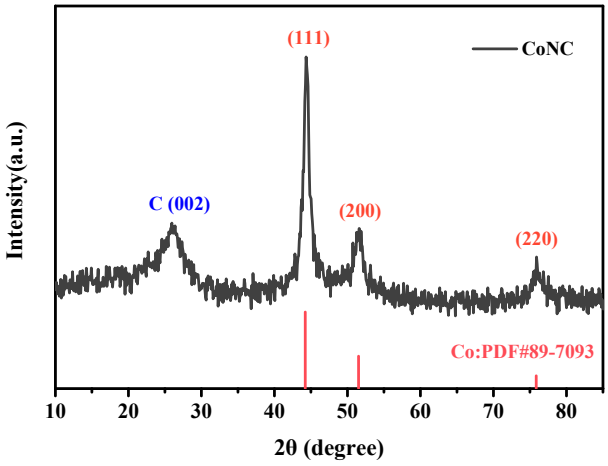

Fig. S2 XRD spectra of CoNC.

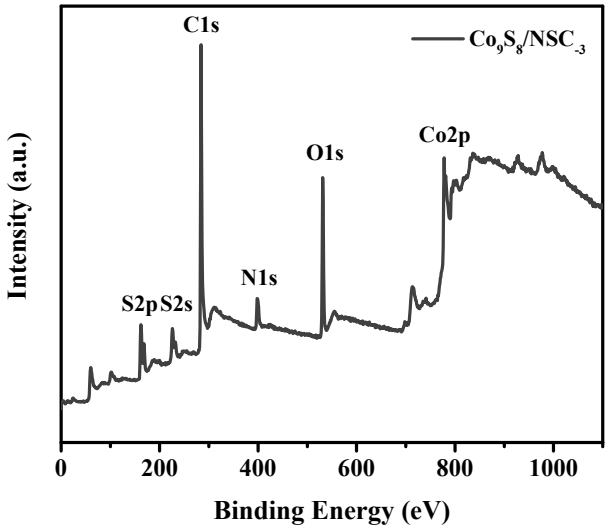

Fig. S3 XPS survey spectrum of Co_9S_8/NSC_{-3}.

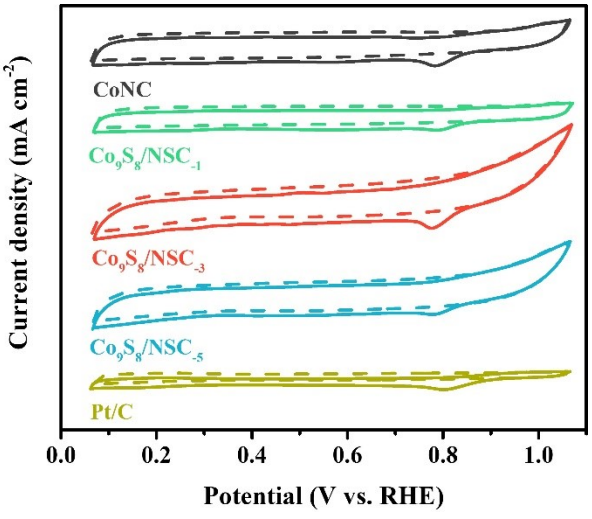

Fig. S4 CV curves in N_2-/O_2-saturated 0.1 M KOH solution.

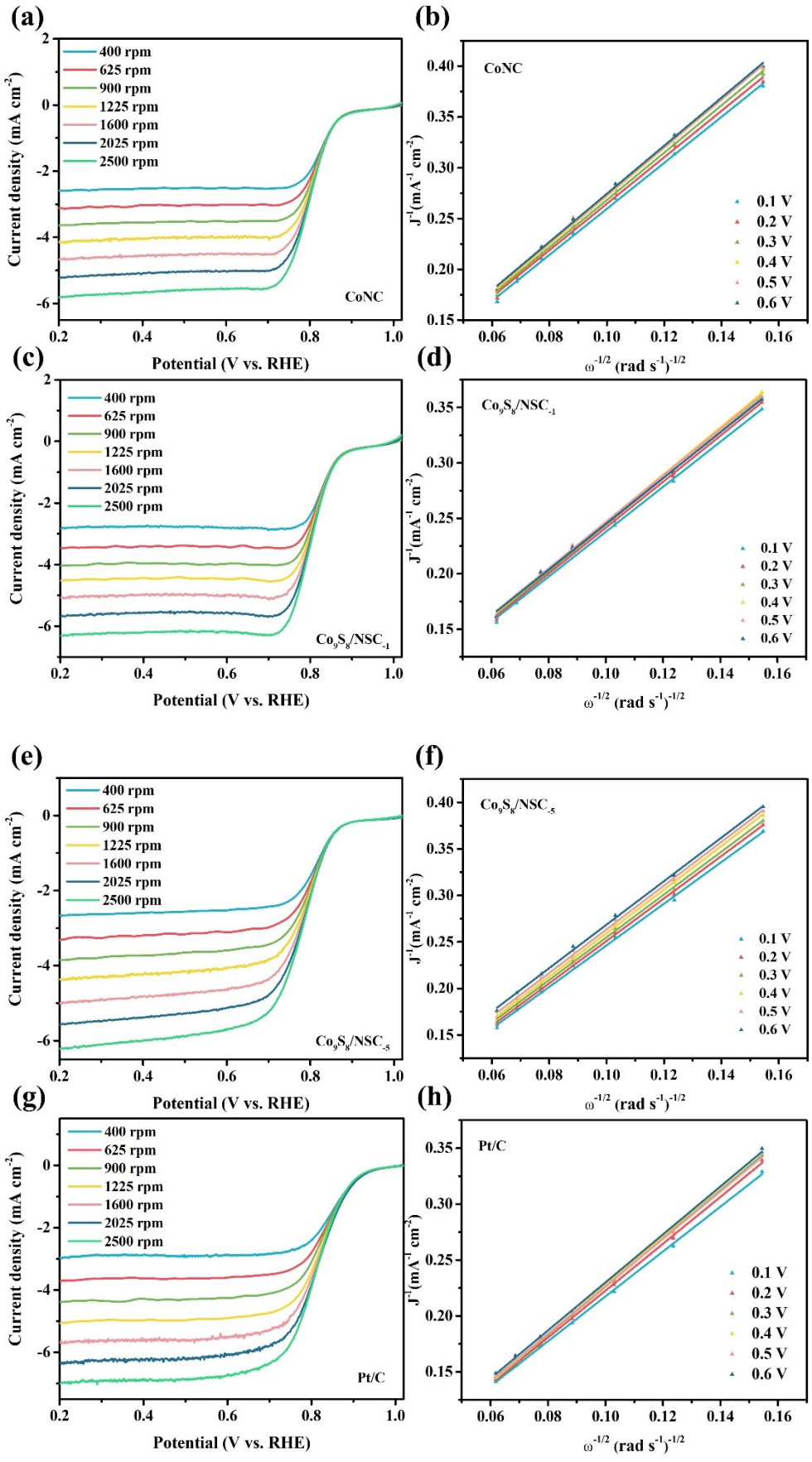

Fig. S5 A series of LSV curves and the corresponding K-L plots of (a, b) CoNC, (c, d)

Co_9S_8/NSC$_{-1}$, (e, f) Co_9S_8/NSC$_{-5}$ and (g, h) Pt/C.

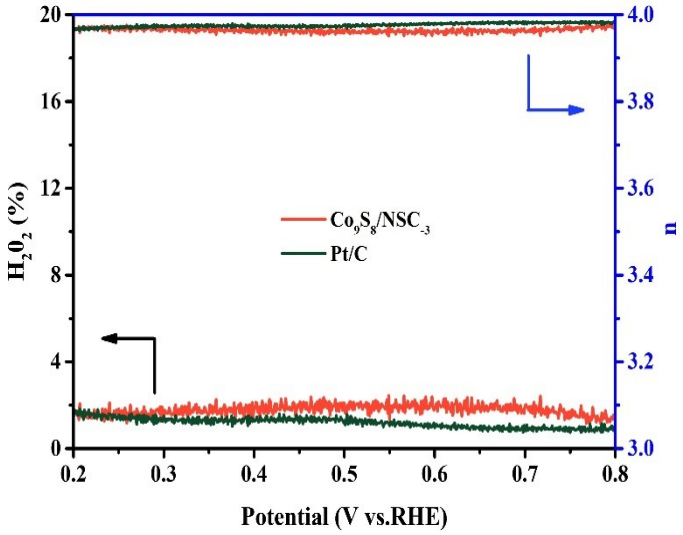

Fig. S6 RRDE measurements.

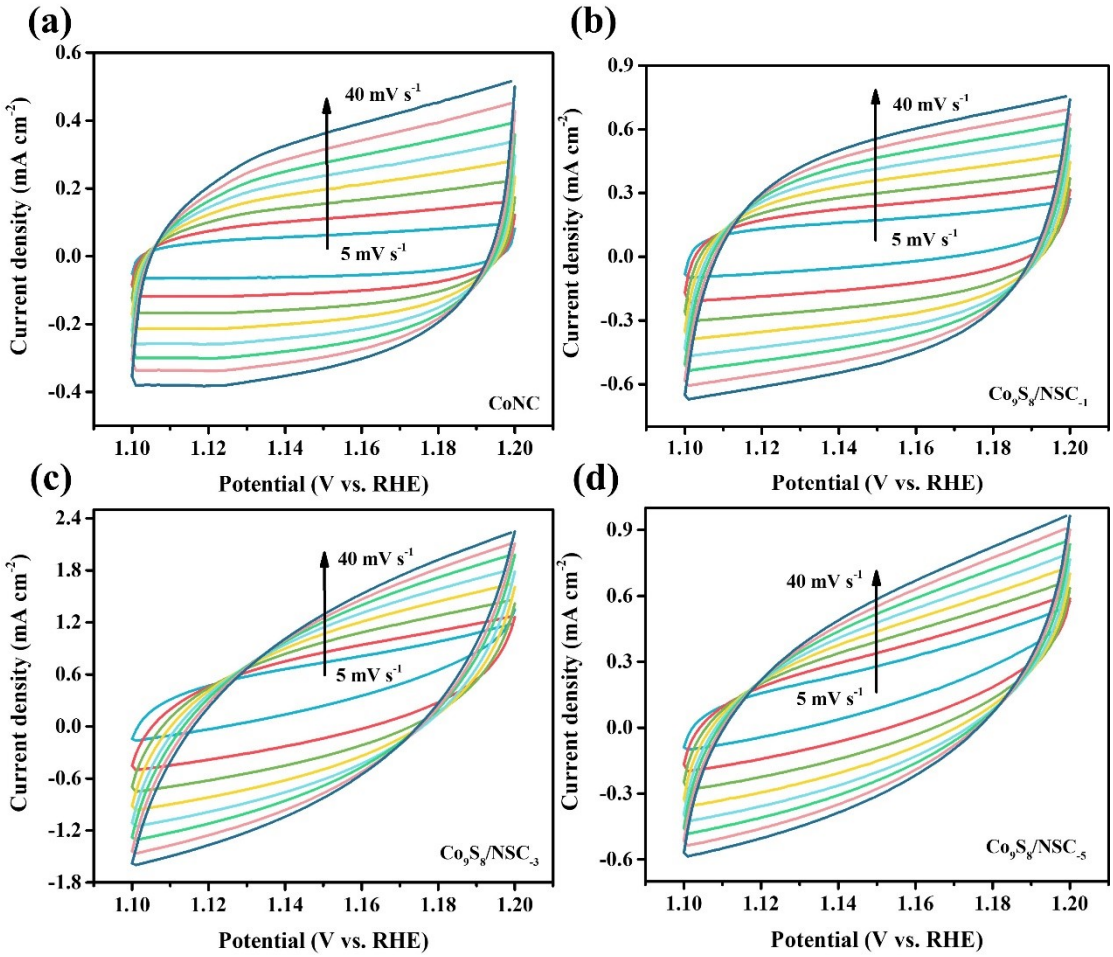

Fig. S7 CV curves at the scan rates of 5, 10, 15, 20, 25, 30, 35, and 40 mV s^{-1} of prepared catalysts: (a) CoNC, (b) Co_9S_8/NSC$_{-1}$, (c) Co_9S_8/NSC$_{-3}$, (d) Co_9S_8/NSC$_{-5}$.

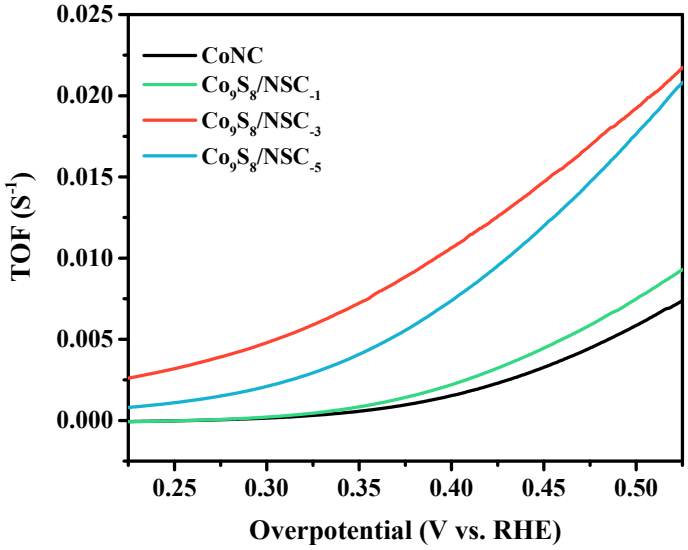

Fig. S8 TOFs calculated at various overpotentials.

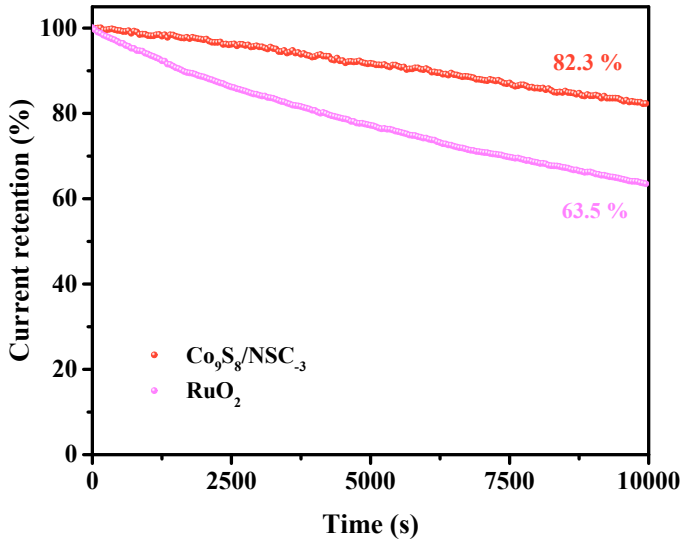

Fig. S9 The i-t curves for Co_9S_8/NSC_{-3} and RuO_2 catalysts.

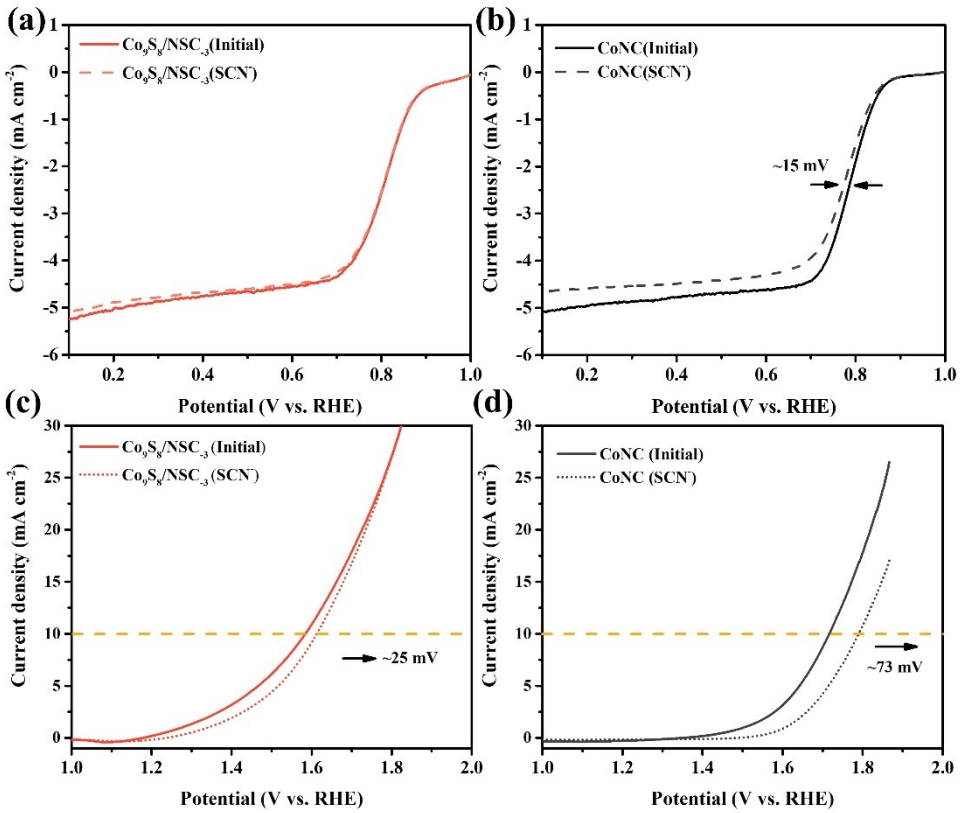

Fig. S10 ORR polarization curves of (a) Co_9S_8/NSC_{-3} and (b) CoNC and OER polarization curves of (c) Co_9S_8/NSC_{-3} and (d) CoNC recorded in 0.1 M KOH with or without poisoning by 10 mM SCN^-.

Table S1: The atomic percentage of each element derived from XPS investigations.

Sample	C (at %)	N (at %)	O (at %)	S (at %)	Co (at %)
Co_9S_8/NSC_{-3}	62.31	7.06	13.84	10.01	6.45

Table S2: Electrocatalytic performance of recently reported other well-developed Co_9S_8-based bifunctional electrocatalysts for ORR and OER in 0.1M KOH.

Catalyst	ORR performance vs RHE			OER performance vs RHE	ΔE ($E_{j=10}$-$E_{1/2}$) (V)	Ref.
	E_{onset} (V)	$E_{1/2}$ (V)	J_L (mA cm $^{-2}$)	$E_{j=10}$ (V)		
Co_9S_8/NSC$_{-3}$	0.89	0.82	-5.15	1.58	0.76	This work
Pt/C	0.92	0.83	-5.61	/	0.77	This work
RuO_2	/	/	/	1.60		
Co_9S_8/S-CNTs	/	0.81	/	1.561	0.751	Carbon, 2019, 144: 259-268.
Co_9S_8@CT-800	0.92	0.86	/	1.62	0.76	J. Mater. Chem. A. 2018, 6(14): 5935-5943.
Co/S/N-800	0.912	0.831	/	1.591	0.76	ChemSusChem, 2019, 12: 383-95.
$FeCo_8S_8$ NS/rGO	/	0.79	/	1.56	0.77	ACS nano 2020, 14(8): 10438-10451.
Co_9S_8/CD@NSC	/	0.84	/	1.62	0.78	ACS Appl. Mater. Interfaces, 2019, 11(15): 14085-14094.
CE-Co_9S_8@N, S-CM	/	0.88	/	1.66	0.78	Catal. Sci. Technol, 2019, 9(20): 5757-5762.
Co_9S_8@TDC-900	/	0.78	-5.45	1.56	0.78	J. Mater. Chem. A, 2019, 7(13): 7389-7395.

Cu-Co_9S_8-NHCS$_{-1}$	0.88	0.772	-5.25	1.56	0.788	J. Alloys Compd. 2022,921: 166076.
Co_9S_8@NSCM	0.97	0.81	-5.11	1.60	0.79	Nanoscale, 2018, 10(5): 2649-2657.
CoS_X@PCN/rGO	0.89	0.78	/	1.57	0.79	Adv. Energy Mater, 2018, 8(1): 1701642.
Co_9S_8/N, P-APC	0.89	0.78	/	1.593	0.813	Carbon, 2019, 144: 557-566.
CoS_2 (400)/N, S-GO	0.97	0.79	/	1.61	0.82	Small, 2016, 12: 1359.
Co_9S_8/NSG-700	0.92	0.79	-4.59	1.61	0.82	Nano-Micro Lett, 2019, 11(1): 4.
IOSHs-NSC-Co_9S_8	0.92	0.82	-5.35	1.64	0.82	Appl. Catal. B, 2020, 260: 118209.
Co_9S_8/GN-0.02	0.93	0.80	-6.4	1.68	0.88	ACS Appl. Mater. Interfaces, 2020, 12(34): 38202-38210.
Co/Co_9S_8/rGO/MWCNT-800	0.946	0.776	-5.54	1.665	0.89	Inorg. Chem. Front, 2019, 6(9): 2558-2565.

References

1 Y. Liu, K. Sun, X. Cui, B. Li and J. Jiang, *ACS Sustainable Chem. Eng.*, 2020, **8**, 2981-2989.

2 Z. Lei, Y. Tan, Z. Zhang, W. Wu, N. Cheng, R. Chen, S. Mu and X. Sun, *Nano Res.*, 2020, **14**, 868-878.

3 Y. Lian, K. Shi, H. Yang, H. Sun, P. Qi, J. Ye, W. Wu, Z. Deng and Y. Peng, *Small*, 2020, **16**, 1907368.

4 Y. Tian, L. Xu, J. Qian, J. Bao, C. Yan, H. Li, H. Li and S. Zhang, *Carbon*, 2019, **146**, 763-771.

5 F. Yuan, Z. Liu, G. Qin and Y. Ni, *Dalton Trans*, 2020, **49**, 15009-15022.

6 S. Zhao, Y. Wang, J. Dong, C.-T. He, H. Yin, P. An, K. Zhao, X. Zhang, C. Gao, L. Zhang, J. Lv, J. Wang, J. Zhang, A. M. Khattak, N. A. Khan, Z. Wei, J. Zhang, S. Liu, H. Zhao and Z. Tang, *Nat. Energy*, 2016, **1**: 1-10.